Separation and Purification Technology 275 (2021) 119169

Contents lists available at ScienceDirect

Separation and Purification Technology

journal homepage: www.elsevier.com/locate/seppur

TiO_2-carbon microspheres as photocatalysts for effective remediation of pharmaceuticals under simulated solar light

Manuel Peñas-Garzón [a,b], Wael H.M. Abdelraheem [b,c], Carolina Belver [a,*], Juan J. Rodriguez [a], Jorge Bedia [a], Dionysios D. Dionysiou [b,*]

[a] Chemical Engineering Department, Universidad Autónoma de Madrid, Campus Cantoblanco, Madrid E-28049, Spain
[b] Environmental Engineering and Science Program, Department of Chemical and Environmental Engineering (ChEE), University of Cincinnati, Cincinnati, OH 45221-0012, USA
[c] Chemistry Department, Faculty of Science, Sohag University, Sohag 82524, Egypt

ARTICLE INFO

Keywords:
TiO_2-carbon microspheres
Lignin
Solar photocatalysis
Pharmaceuticals
Diclofenac
Degradation pathway

ABSTRACT

In this work, novel carbon microspheres supported TiO_2 nanoparticles were prepared for the degradation of pharmaceuticals in water, selecting diclofenac, acetaminophen, and ibuprofen as target pollutants. Lignin, an important biomass byproduct from the paper industry and biorefineries, was transformed in carbon microspheres by a novel approach based on a Fe-activated hydrothermal carbonization followed by pyrolysis at 900 °C. These carbon microspheres were further covered with TiO_2 by a solvothermal treatment. The effects of several parameters including hydrothermal carbonization time and mass ratio (TiO_2:carbon) on the catalytic activity of TiO_2-carbon microspheres were investigated. The results revealed that the combination of long carbonization time and high TiO_2:carbon ratio achieved superior TiO_2-carbon microspheres (Ti2-C20) catalytic performance. Ti2-C20 achieved complete degradation of ibuprofen (5 $mg{\cdot}L^{-1}$) and diclofenac (5 $mg{\cdot}L^{-1}$) within 3 h under solar light and mineralization percentages close to 50%. Moreover, the photocatalytic performance remained high after five reuse cycles and was barely affected by the presence of common inorganic ions in treated wastewater (such as Cl^-, NO_3^- and HCO_3^-). The degradation pathway of diclofenac was proposed, involving C-N bond cleavage, and subsequent hydroxylation and cyclization reactions leading to the formation of aliphatic carboxylic acids. Overall, promising photocatalysts were obtained from a biomass byproduct for effective degradation of pharmaceuticals with the assistance of solar light.

1. Introduction

The presence of pharmaceutical residues in wastewater effluents poses an environmental threat due to their adverse biological activity, affecting their likely reuse (as treated wastewater or "reclaimed" water). Analgesic and anti-inflammatory drugs (e.g., diclofenac, DCF; ibuprofen, IBU; and acetaminophen, ACE) are among the most common commercially distributed pharmaceuticals. They are frequently detected in those effluents at concentration levels above the ecotoxicity endpoints of different organisms (i.e., from a few $ng{\cdot}L^{-1}$ to several $mg{\cdot}L^{-1}$) [1,2]. Conventional treatment technologies used at wastewater treatment plants (WWTPS) can only achieve partial removal (~21–40%) of these compounds [3]. Stimulated by these facts, several treatment methods have been investigated for the removal of pharmaceuticals in water [4]. Among them, advanced oxidation processes (AOPs) proved to be very efficient in the degradation of these contaminants. Solar-driven photocatalysis has gained increasing interest as environmentally friendly and cost-effective potential solution for the abatement of emerging contaminants, including pharmaceuticals and personal care products [5,6].

Titanium dioxide (TiO_2) is the most used semiconductor in photocatalysis due to its established activity and relatively low toxicity compared to other types of photocatalysts [7]. However, the application of TiO_2 nanoparticles in slurry configuration makes the recovery of the photocatalyst difficult [8]. Although anchoring the semiconductor on a support may introduce mass transfer limitations, it is expected to facilitate the postseparation process of the photocatalyst [9–11]. In this respect, carbon spheres have gained increasing interest as supports due to their high structural stability, tunable porosity and particle size [12,13]. The extensive research performed by Titirici et al. [14–16] revealed some of these promising advantages and likely applications

* Corresponding authors.
E-mail addresses: carolina.belver@uam.es (C. Belver), dionysdd@ucmail.uc.edu (D.D. Dionysiou).

https://doi.org/10.1016/j.seppur.2021.119169
Received 30 March 2021; Received in revised form 3 June 2021; Accepted 16 June 2021
Available online 21 June 2021

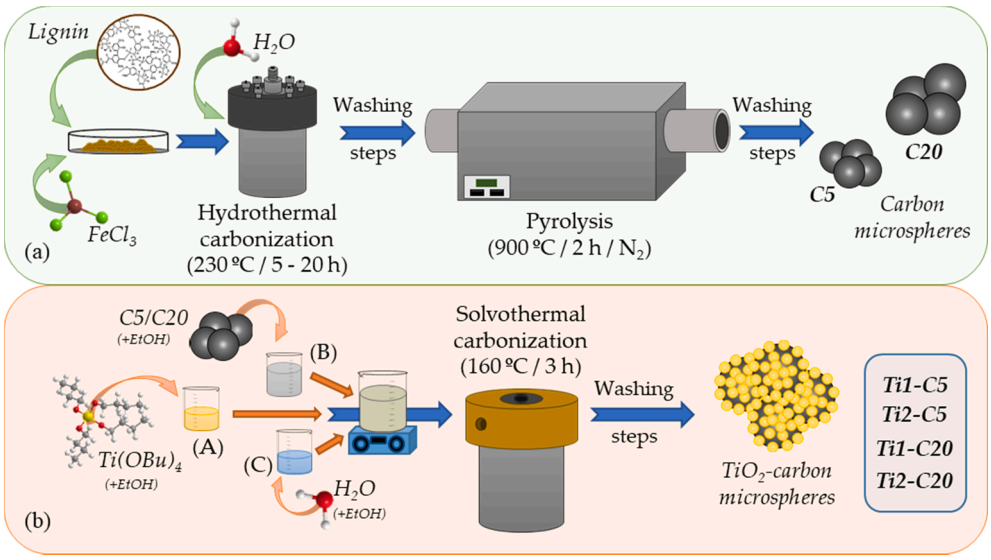

Fig. 1. Schematic diagram for the synthesis of (a) CX and (b) TiY-CX samples.

related to carbon microspheres prepared via hydrothermal carbonization (HTC) of different biomass derivatives (e.g., xylose, furfural or glucose) as carbon sources. However, the use of highly complex molecular carbon precursors has been investigated in less detail. Lignin is an abundant natural polymer and an abundant waste coming from the paper and biorefinery industry, making its valorization a need for environmental sustainability [17,18]. Lignin has been previously used for the preparation of carbon materials such as activated carbons (AC) [19,20], carbon fibers [21,22], templated carbons [23] and even as carbon-dopant [24]. In this sense, lignin has been used for obtaining TiO_2/AC heterostructures with high photocatalytic activity for degradation of pharmaceuticals [25]. More recently, similar TiO_2/AC photocatalysts were prepared via different synthesis routes, and encompassed efficient removal of several pharmaceuticals under a wide range of solution pH [26].

The novelty of this work is the preparation of carbon microspheres via a Fe-based HTC-pyrolysis of lignin, used for the solvothermal synthesis of TiO_2-carbon microspheres heterostructures and tested in the photocatalytic removal of pharmaceuticals. The effect of the HTC holding time and the TiO_2:carbon microspheres mass ratio in the final properties of the heterostructures was investigated. Preliminary studies were assessed with ACE and IBU to identify the heterostructure with the highest photocatalytic performance. After that, the removal of DCF was investigated under different operating conditions (pH, presence of inorganic ions and reuse) and the degradation pathways of this compound were proposed based on identified reaction byproducts.

2. Materials and methods

2.1. Chemicals and reagents

Lignin was purchased from LignoTech Iberica S.A. $FeCl_3{\cdot}6H_2O$ (≥97%) and ethanol (EtOH, 96%) were both obtained from Panreac. Titanium tetrabutoxide ($Ti(OBu)_4$; ≥97%), and the target contaminants, i.e., acetaminophen (ACE, $C_8H_9NO_2$, ≥99%), ibuprofen (IBU, $C_{13}H_{18}O_2$, ≥98%) and diclofenac sodium salt (DCF, $C_{14}H_{10}Cl_2NNaO_2$) were purchased from Sigma Aldrich. $NaHCO_3$ (>99%, Fischer Chemical), NaCl (>99%, Sigma Aldrich) and $NaNO_3$ (>99%, Sigma Aldrich) were used to study the impact of inorganic anions on the degradation process. Acetic acid (≥99%, Sigma Aldrich) and acetonitrile (ACN, HPLC grade, Scharlau) were used as mobile phases for liquid chromatography. Ultrapure deionized water (18.2 MΩ·cm) was used throughout the entire study.

2.2. Synthesis of the photocatalysts

2.2.1. Preparation of carbon microspheres

Fig. 1a depicts a schematic diagram of carbon microspheres (CX) preparation. Lignin and $FeCl_3$ (1:2 mass ratio) were mechanically mixed for 15 min at room temperature until a homogeneous yellow-brown powder was obtained. In this respect, the addition of iron ions has been reported to accelerate the hydrolysis of lignin, mainly via dehydration and decarbonylation [27]. Once the mixture was prepared, 15 mL of ultrapure water were added and the suspension was magnetically stirred for 10 min. It was subsequently placed in a Parr 4740 High Pressure Vessel and then submitted to hydrothermal carbonization (HTC) at 230 °C in an oven for 5 and 20 h. After cooling to room temperature, the solid was separated using Nylon filters (0.45 μm, Scharlau), washed with ultrapure water until obtaining neutral filtrate pH, and dried at 60 °C for 24 h. The solid product was further heat-treated in a horizontal stainless-steel tubular furnace at 900 °C (ramp rate of 10 °C·min^{-1}) for 2 h under inert atmosphere (N_2, 150 cm^3 STP·min^{-1}). The resulting materials were washed with water, filtered, and dried overnight as previously indicated. The final samples were denoted as "CX", where "X" corresponding to the HTC holding time (i.e., 5 and 20 h).

2.2.2. Synthesis of TiO_2-carbon microspheres.

The TiO_2-carbon microsphere heterostructures (TiY-CX) were prepared by a solvothermal procedure (Fig. 1b), following a previously described method [25]. Typically, 1 mL of $Ti(OBu)_4$ was diluted in 15 mL of EtOH (solution A), meanwhile predefined amount of CX was suspended in 45 mL of EtOH (suspension B) under continuous stirring. The amount of CX followed a 1:1 or 2:1 mass ratio of TiO_2:CX. The solution A was added to the suspension B and stirred for 5 min. A solution (C), consisting of 3 mL of ultrapure water diluted in 15 mL of EtOH, was then added dropwise to the previous mixture to promote the hydrolysis of the $Ti(OBu)_4$, while maintaining the stirring for 5 min. Subsequently, the mixture was transferred to a 125 mL Teflon-lined stainless-steel autoclave and treated at 160 °C for 3 h in a Memmert UN30 oven. The resulting solid was centrifuged at 5300 rpm for 10 min, washed once with EtOH and four times with ultrapure water and finally dried at 60 °C overnight. The obtained samples were denoted as TiY-CX, where "Y" represents the TiO_2 to carbon microspheres mass ratio (i.e., 1 or 2).

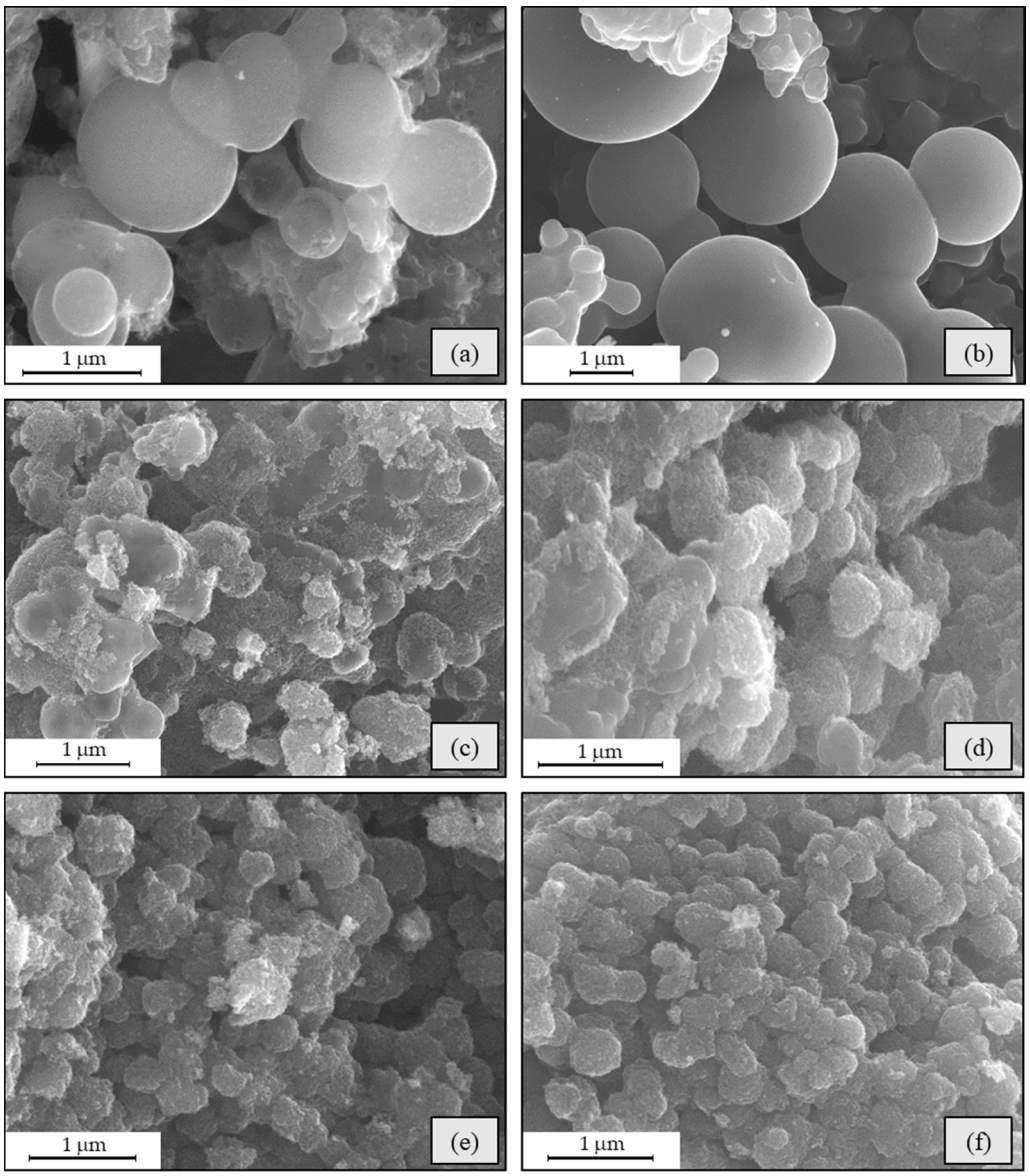

Fig. 2. SEM micrographs of (a) C5, (b) C20, (c) Ti1-C5, (d) Ti1-C20, (e) Ti2-C5 and (f) Ti2-C20.

2.3. Characterization of the heterostructures

A Quanta 3D Field Emission Gun (FEG) microscope (FEI Co.) was used to observe the morphology of the samples by scanning electron microscopy (SEM). The SEM images were used to determine the mean particle size of the synthesized microspheres with the ImageJ software. X-ray diffraction (XRD) patterns were recorded in the 2θ range of (15–70°) at a scan rate of $5°{\cdot}min^{-1}$, by using a Bruker D8 diffractometer (Cu-Kα source, $\lambda = 0.15406$ nm). The porous texture of the heterostructures was assessed from the N_2 adsorption–desorption isotherms (−196 °C) using a Micromeritics TriStar 123 static volumetric equipment. The samples were previously degassed under vacuum at 150 °C for 16 h in a Florprep 060 Micromeritics equipment. Specific surface area (S_{BET}) was determined by the Brunauer-Emmett-Teller (BET) method [28], while external or non-microporous surface area (S_{EXT}) and micropore volume (V_{MP}) were estimated by the *t*-plot method [29]. Total pore volume (V_T) was calculated as the amount of adsorbed nitrogen (expressed as liquid) at a relative pressure (P/P_0) of 0.99. A Shimadzu 2600 UV–vis spectrophotometer was used to obtain the UV–vis diffuse reflectance spectra (UV–vis DRS) against $BaSO_4$ as reference material. The band gap (E_g) values were estimated from UV–vis DRS spectra using the Tauc plot method [30] considering the synthesized photocatalysts as indirect semiconductors [31]. A PHI VersaProbe II spectrometer using Al Kα X-ray (1486.68 eV) as excitation source was used to record the spectra of X-ray photoelectron spectroscopy (XPS) analysis. The C1s peak was set at 284.5 eV and used as internal reference. The pH drift method was used to determine the pH at the point of zero charge (pH_{PZC}) [32]. A Varian Cary Eclipse fluorescence spectrophotometer was used to obtain the photoluminescence (PL) spectra of the samples at $\lambda_{excitation}$ of 240 nm. Thermogravimetric analysis in air ($100\ mL{\cdot}min^{-1}$) up to 900 °C (at $10\ °C{\cdot}min^{-1}$) were carried out using a Discovery SDT 650 (TA Instruments).

2.4. Photocatalytic experiments

The photocatalytic experiments were performed for 3 h under simulated solar light (Newport Xenon lamp, $500\ W{\cdot}m^{-2}$). A Light correction filter (Newport FSQ-KG5, restrained $\lambda \leq 350$ nm) was used to obtain a light spectrum similar to solar radiation. The distance from the filters to the surface of the solution was fixed at 22 cm. An aqueous solution (50 mL) containing predefined concentration of the contaminant was placed in a 100 mL borosilicate petri dish with a quartz cover

and kept under continuous stirring for 3 h. For all experiments, unless otherwise stated, 5 mg·L^{-1} initial target compound concentration was used in presence of 250 mg·L^{-1} of photocatalyst. A set of previous experiments were conducted to determine the photocatalytic performance of solar light/TiY-CX system for the degradation of ACE and IBU in aqueous solution at natural pH (i.e., 6.9 and 7.1 for ACE and IBU, respectively). The catalyst with the highest photocatalytic performance was further used to comprehensively study the degradation of DCF in water. Adsorption tests (in absence of light) were carried out prior to the photocatalytic runs. Unless otherwise stated, DCF degradation experiments were performed at the natural solution pH (6.0).

Aliquots of 400 μL were taken at different time intervals and centrifuged at 15,000 rpm for 15 min to separate the catalyst and the concentration of the target contaminant was determined by High Performance Liquid Chromatography (HPLC), using an Agilent 1100 Series HPLC and a Supelco C18 column (150 × 2.1 mm, 5.0 μm). A mixture of A: ACN and B: acetic acid 0.1% (v/v) was used as a mobile phase to elute ACE using a gradient method (A/B changed from 10/90 ratio (v/v) to 40/60 in 10 min, setting the flow rate to 0.7 mL·min^{-1}, column temperature at 40 °C and λ = 246 nm as the detection wavelength), while isocratic methods were used for the analysis of IBU (50/50, 0.7 mL·min^{-1}, 40 °C, λ = 220 nm) and DCF (45/55, 0.8 mL·min^{-1}, 35 °C, λ = 276 nm). Total organic carbon (TOC) was measured with a Shimadzu TOC-L analyzer. The effect of natural inorganic anions on the photocatalytic performance of Ti2-C20 for DCF degradation was studied by amending initial solution with Cl^- (2.50 mM), NO_3^- (0.83 mM) or HCO_3^- (3.07 mM). These concentrations were chosen as representative maximum values in wastewater after reclamation treatment [33]. A Bruker Maxis II equipment with electrospray ionization (ESI positive) was used for the identification of the DCF degradation byproducts by liquid chromatography and electrospray ionization-mass spectrometry (LC/ESI-MS) using the following conditions: *m/z* range from 50 to 3000, capillary voltage of 3500 V, end plate offset of 500 V and dry heater at 200 °C with a gas flow of 6.0 L·min^{-1}. A Metrohm 790 IC chromatograph with a Metrosep A Supp 5 (250 mm × 4 mm) column (Metrohm) was used for the detection and quantification of low molecular weight carboxylic acids as well as inorganic ions using corresponding standards solutions. Elution was carried out with Na_2CO_3/$NaHCO_3$ aqueous mixture (3.2 mM/1.0 mM) at a flow rate of 0.7 mL·min^{-1} and H_2SO_4 (100.0 mM) as suppressor. All experiments were performed in duplicate and average values were calculated. A third experiment was performed in case of more than 5% difference of the duplicates.

3. 3. Results and discussion

3.1. Material characterization

Fig. 2 depicts SEM images of carbon microspheres and TiO_2-carbon heterostructures. Generally, carbon spheres consisted of interconnected microspheres with different sizes. A comparison between C5 (Fig. 2a) and C20 (Fig. 2b) indicates that higher HTC holding time leads to larger carbon microspheres, i.e., particle diameter changed from 0.9 ± 0.4 μm in C5 to 1.9 ± 0.8 μm in C20. The formation of spherical structures from lignin is considered a difficult process due to its heterogeneous aromatic macro-biopolymer structure. Titirici et al. [14] and Falco et al. [34] reported that the HTC of monosaccharides mainly led to the formation of well dispersed/separated carbon spheres. When more complex carbon precursors (e.g., lignocellulosic biomass) were used, partially interconnected carbon microspheres with some domains of aggregated spherical particles were obtained. This has been attributed to the presence of lignin, a more structurally stable material than cellulose. The complexity in preparation of carbon spheres using lignin as carbon precursor has been discussed in few published reports on the topic, as collected in Table S1 of the Supplementary Information. Historically, polymerization is mostly used for the synthesis of carbon spheres and usually results in the formation of micron-size carbon particles i.e., (1.3–350 μm).

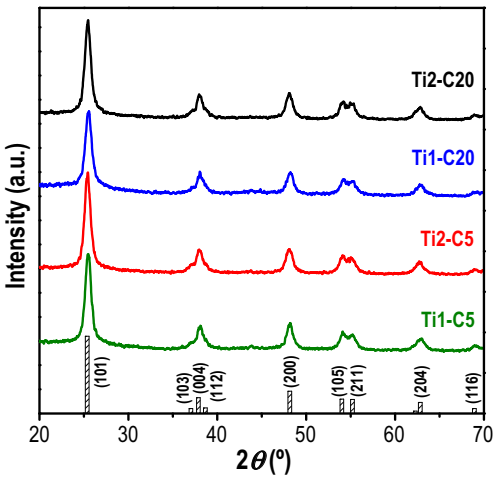

Fig. 3. XRD patterns of the synthesized heterostructures. The diffraction peaks of anatase phase (JCPDS 21–1272) are included.

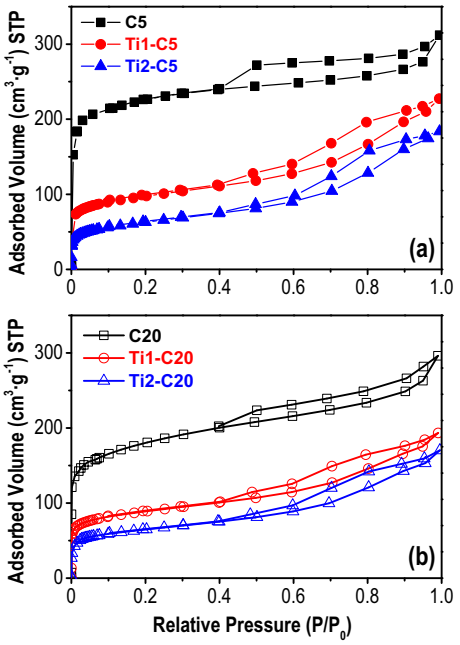

Fig. 4. N_2 adsorption-desorption isotherms (-196 °C) of the (a) C5- and (b) C20-derived heterostructures.

Fig. 2 (c)-(f) reveals the loss of carbon smooth surface due to the deposition of TiO_2 nanoparticles. Uneven distribution of those particles and incomplete coating of carbon spheres were observed in the samples with lower TiO_2 content (i.e., Ti1-C5 and Ti1-C20), while the distribution of TiO_2 particles was more uniform in Ti2-C5 and Ti2-C20 heterostructures, being the carbon spheres completely coated with TiO_2. These results, accordingly, suggest that the synthesis of ideal TiO_2-carbon heterostructures requires a minimum TiO_2:carbon mass ratio of 2:1 to ensure an appropriate dispersion of TiO_2 on the microspheres surface.

Fig. 3 depicts the XRD patterns of the synthesized photocatalysts, as well as the characteristic diffraction peaks of the anatase phase of TiO_2 (JCPDS 21-1272). All prepared TiO_2-carbon microspheres encompassed pure anatase structure, i.e., the most photoactive crystalline phase of TiO_2 due to its higher electron mobility [31,35]. Similar anatase-type TiO_2 has been previously reported anchored on an activated carbon by solvothermal synthesis without further calcination at high temperature

Table 1
Porous texture, bandgap values and pH_{PZC} of carbon microspheres and TiO_2-carbon heterostructures.

Sample	S_{BET} ($m^2 \cdot g^{-1}$)	S_{EXT} ($m^2 \cdot g^{-1}$)	V_T ($cm^3 \cdot g^{-1}$)	V_{MP} ($cm^3 \cdot g^{-1}$)	E_g (eV)	pH_{PZC}
C5	697	91	0.483	0.315	n.d.	n.d.
Ti1-C5	331	165	0.352	0.078	3.36	6.74
Ti2-C5	219	148	0.284	0.032	3.30	6.79
C20	603	167	0.458	0.209	n.d.	n.d.
Ti1-C20	301	139	0.299	0.076	3.34	6.68
Ti2-C20	221	127	0.263	0.044	3.30	6.70

S_{BET}, specific surface area; S_{EXT}, external surface area; V_T, total pore volume; V_{MP}, micropore volume; E_g, band gap of the photocatalysts; and pH_{PZC}, pH at point of zero charge (drift method). n.d.: not determined.

[25]. Nitrogen adsorption-desorption isotherms of the synthesized carbon microspheres and TiO_2-carbon heterostructures are shown in Fig. 4, and the characterization of the porous texture is summarized in Table 1. All isotherms belong to type IV with H4 hysteresis cycles (according to IUPAC classification [36]), typical of porous materials with development of both micro- and mesoporosity. Since the same pyrolysis process was used for the synthesis of C5 and C20, the textural differences of both samples were ascribed to the initial HTC conditions. The decrease of S_{BET}, from 697 $m^2 \cdot g^{-1}$ in C5 to 603 $m^2 \cdot g^{-1}$ in C20, can be attributed to partial coalescence of micropores in C5 into mesopores in C20 microspheres due to the longer HTC treatment time. This fact was also supported by the reduction of V_{MP} as increasing the HTC time. The S_{BET} values of both C5 and C20 were considerably higher than those reported for counterparts prepared from lignin by different synthesis procedures (Table S1). The surface development was probably due to the activation effect of residual $FeCl_3$ from the HTC step during the pyrolysis step, as previously described for the preparation of $FeCl_3$-activated carbons [37]. The deposition of TiO_2 on the carbon microspheres caused a significant reduction of the corresponding S_{BET} and V_{MP} values (Table 1), due to partial blockage of micropores. However, these values were higher than those reported by Wu et al. [38] for TiO_2-carbon spheres prepared from sucrose as carbon precursor, which can be explained by the absence of activation step in their synthesis method.

Fig. 5a shows the light absorption spectra of the different synthesized heterostructures and the counterpart of bare TiO_2 for comparison. Two different regions were identified: (i) UV ($\lambda < 400$ nm), corresponding mainly to the radiation absorbed by TiO_2, and (ii) visible region ($400 < \lambda < 750$ nm) ascribed to light absorption by the characteristic dark gray-colored carbon support. The E_g values, around 3.3 eV (Table 1), were all estimated from the Tauc plot (Fig. 5b and c) using the baseline approach to consider the contribution of light absorbed by the carbon support [39]. Those band gaps, fairly close to that of bare TiO_2 (3.33 eV, Fig. 5c), suggested that the interaction between the carbon microspheres and the TiO_2 enhanced the absorption of light in the visible range, but did not modify the band gap.

Fig. 6 shows the XPS spectra of Ti2-C20 as reference material. The full spectra (Fig. 6a) confirmed the presence of C, Ti, and O atoms in the surface of the heterostructure. The deconvolution of C 1s peaks (Fig. 6b) revealed different surface carbon species mainly related to the carbon microspheres. The main contribution can be attributed to the existence of aromatic sp^2 C=C (284.5 eV, 48.6%) [38], followed by aliphatic sp^3 C-C (285.7 eV, 25.7%) and oxidized carbon forms as C-O-C / C-OH (286.4 eV, 20.5%) and O-C-O (289.5 eV, 5.2%) [40–42], which can be probably formed during the synthesis of carbon microspheres. The absence of the peak around 282 eV suggested that C was not incorporated in the TiO_2 lattice, as previously reported by Zhao et al. [43]. XPS spectrum of Ti 2p is depicted in Fig. 6c. The peaks at binding energy 459.4 and 465.1 eV were ascribed to Ti-O bonds (Ti^{4+} $2p_{3/2}$ and $2p_{1/2}$ due to spin-orbital, respectively). However, these values are slightly higher than those reported for pure TiO_2 anatase phase [44], suggesting a different environment compared to pure anatase as reported by An et al. [45], probably due to the synthesis of TiO_2 particles on the surface of the carbon microspheres. Regarding the O 1s spectrum (Fig. 6d), the deconvolution yielded two main peaks at 530.6 eV (70.9%) and 531.5 eV (29.1%) assigned to oxygen bonding (Ti-O-Ti and -OH groups, respectively [42,46]). The XPS spectrum recorded at low binding energies allows the estimation of the maximum valence band (Fig. 6e), located at 3.57 eV. Considering the band gap value determined above for Ti2-C20 (E_g = 3.30 eV, Table 1), the minimum conduction band of the photocatalyst would lie at 0.27 eV, as depicted in Fig. 6f.

3.2. Photocatalytic performance

3.2.1. Removal of pharmaceuticals

The photocatalytic performance of the synthesized heterostructures was initially evaluated in preliminary studies in the removal of ACE and IBU (Fig. S1 of the Supplementary Information) under simulated solar light. Adsorption experiments of contaminants, under dark conditions, were firstly performed showing their negligible affinity to the tested photocatalysts. This was likely due to the weak electrostatic interaction between ACE and IBU with the electrically uncharged surface of the heterostructures ($pH_{PZC} \approx 6.7$–6.8, Table 1 and Fig. S2) at natural pH. The contaminants exhibited marginal direct photolysis by solar light, while a noticeable reduction of their concentration was achieved in the

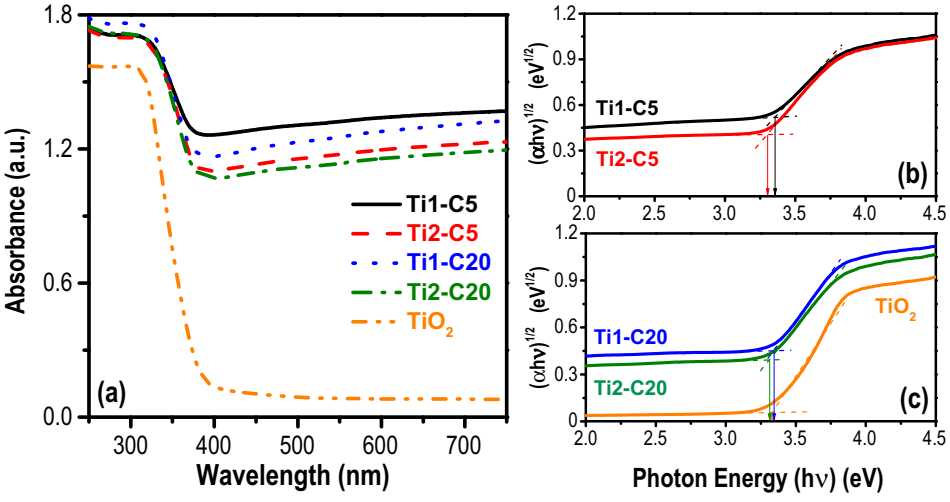

Fig. 5. (a) UV–vis diffuse reflectance spectra (UV–vis DRS) of synthesized heterostructures, and Tauc plots of: (b) Ti1-C5 and T2/C5, (c) Ti1-C20 and T2-C20. (Extrapolations are depicted by dash lines). UV–vis DRS and Tauc Plot of bare TiO_2 has been included for comparison.

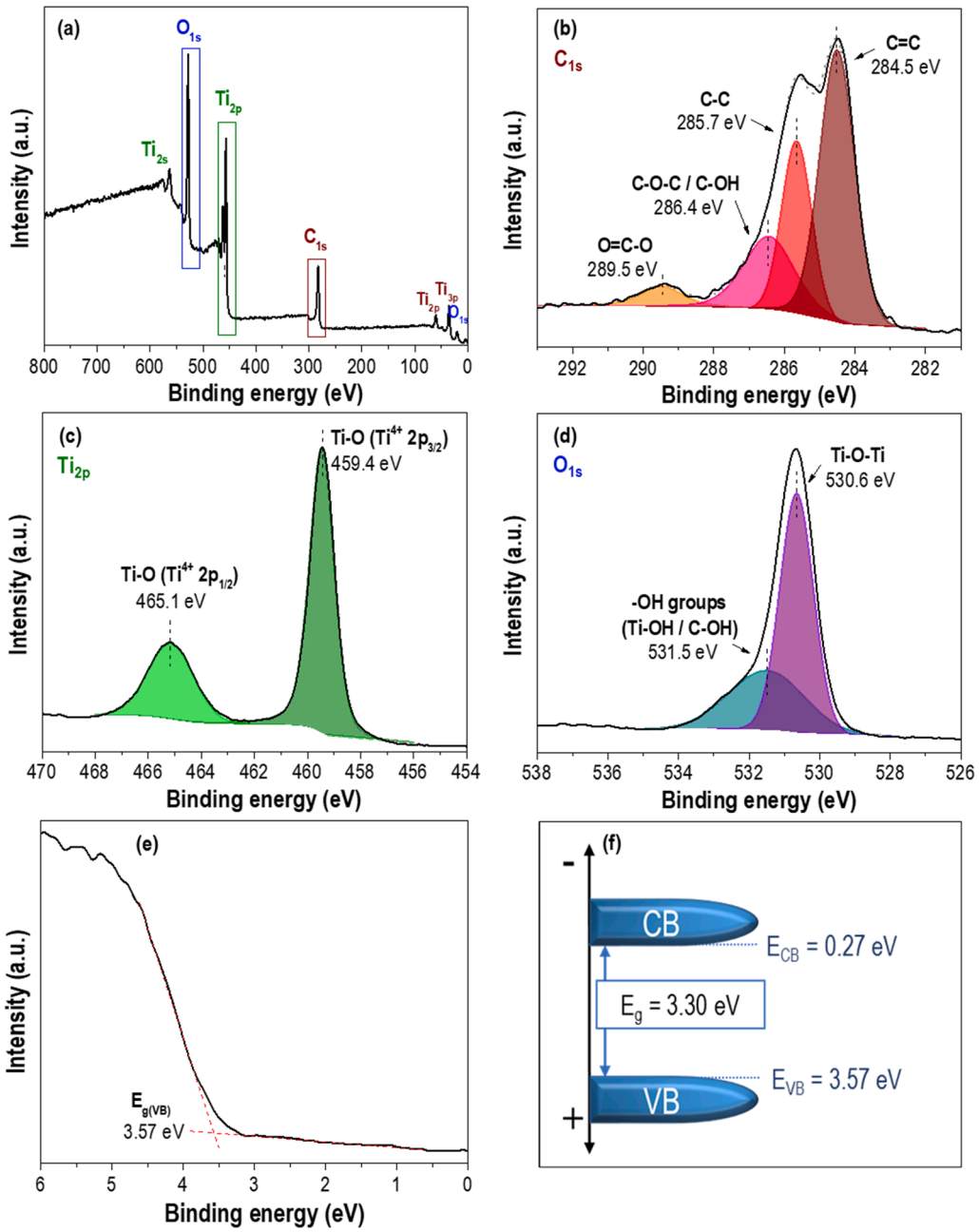

Fig. 6. XPS surface analysis of Ti2-C20: (a) full spectra, (b-d) high-resolution XPS spectra of C 1s, Ti 2p and O 1s peaks, (e) XPS spectrum at low binding energies for the estimation of the maximum valence band, and (f) proposed band structure of Ti2-C20.

presence of the synthesized photocatalysts. Ti2-C20 catalyst yielded the highest apparent photonic efficiencies (ξ, 2.78 and 8.98 einstein^{-1} for ACE and IBU, respectively) as collected in Table S2. In terms of contaminants conversion and mineralization, approximately 65 and 95% reduction of the ACE and IBU concentration was respectively achieved after 3 h, accompanied of about 45% TOC decrease in both cases (Fig. S1). Ti2-C20 and Ti2-C5 yielded comparable photocatalytic degradation of the target contaminants due to their analogous structural (Table 1) and optical properties based on PL spectra (Fig. S3). It is noteworthy that the highest absorption of visible light in the T1-C5 and Ti1-C20 samples, as observed from the UV–vis DRS, was not necessarily related to a better photocatalytic activity because of the unchanged band gap of the semiconductor. Given the superior photocatalytic performance and photonic efficiency of Ti2-C20, it was chosen to study the removal of DCF as target pharmaceutical, including identification of transformation products and elucidation of reaction pathway.

Fig. 7 shows the time course of DCF at two initial concentrations (i.e., 5 and 8 mg·L^{-1}) by using Ti2-C20. In this case, significant amounts of DCF were adsorbed onto the photocatalyst under dark conditions after 90 min. No further adsorption was observed between 90 and 120 min. The much higher affinity of Ti2-C20 for DCF can be due to the electrostatic interaction between the anionic DCF species (pH (6.0) > pKa (4.2)) and the slightly positive surface of Ti2-C20 (pH (6.0) < pH_{PZC} (6.7)) at the 6.0 testing pH. Negligible degradation of the pharmaceutical (<1%) was observed in the absence of photocatalyst. Almost complete removal of DCF (ξ = 17.65 einstein^{-1}, Table S2) was achieved after 3 h under simulated solar light, with 56% and 42% TOC reduction. Scavenger experiments, shown in Fig. S4, suggested that direct holes (h^+) would be the major oxidizing species in this process. The photocatalytic removal of DCF by Ti2-C20 was investigated over a wide range of pH (i.e., 3–9, Fig. S5) showing an effective DCF conversion at different initial pH. Other relevant studies regarding the removal of DCF using

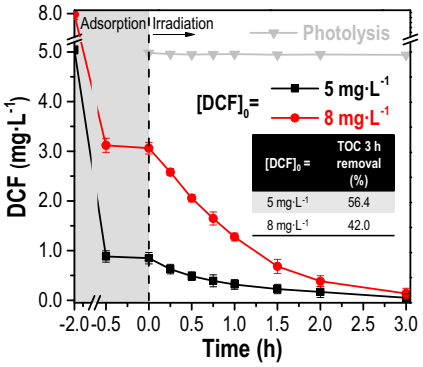

Fig. 7. Time-course of DCF concentration with Ti2-C20 (250 mg·L^{-1}). TOC removal after 3 h of photocatalytic treatment is also included. pH_0 = 6.0.

TiO_2-supported photocatalysts under solar light are summarized in Table S3, demonstrating the adequate performance of this type of systems for the abatement of DCF under solar light.

3.2.2. *Effect of inorganic anions*

The presence of inorganic species such as Cl^-, NO_3^- and HCO_3^- was reported to interfere with the role of reactive oxygen species, especially $HO^\bullet$, for the degradation of organic contaminants in water [47]. Thus, individual DCF degradation tests were carried out with Ti2-C20 in presence of the above inorganic anions at environmentally relevant concentration (see Section 2.4 for more details). Cl^- and NO_3^- showed a negligible impact on the photocatalytic performance (Fig. 8a). The same conclusion was reported with other TiO_2-based photocatalysts [33,41,48], explained by the formation of less reactive radical species (e.g., $Cl^\bullet$ and $NO_3^\bullet$) than $HO^\bullet$, in addition to the minor contribution of $HO^\bullet$ for DCF degradation in those systems. On the other side, the presence of HCO_3^- increased the initial solution pH to 9.1 and led to some enhancement of the photocatalytic performance, as can be seen in Fig. 8b. Abdelraheem et al. reported a considerable quenching of $HO^\bullet$ in presence of HCO_3^- in DCF degradation using N and B-codoped TiO_2, and revealed the formation of carbonate radical ($CO_3^{\bullet-}$) due to chemical interaction between the hydroxyl radical and carbonate species [33]. According to Huang et al. [49], $CO_3^{\bullet-}$ possesses lower reactivity than $HO^\bullet$ for organic compounds, although it has higher selectivity towards phenolic and aromatic amine fractions as in the case of DCF.

3.2.3. *Catalyst reusability*

Fig. 9 depicts the DCF degradation profile over five sequential photocatalytic experiments with Ti2-C20. The photocatalyst was recovered by centrifugation after each reaction cycle, washed with methanol and dried at 100 °C. The photocatalytic activity slightly decreased upon five successive cycles, to 80% vs the 94% removal achieved in the first cycle. A comparison between SEM micrographs of the as-prepared

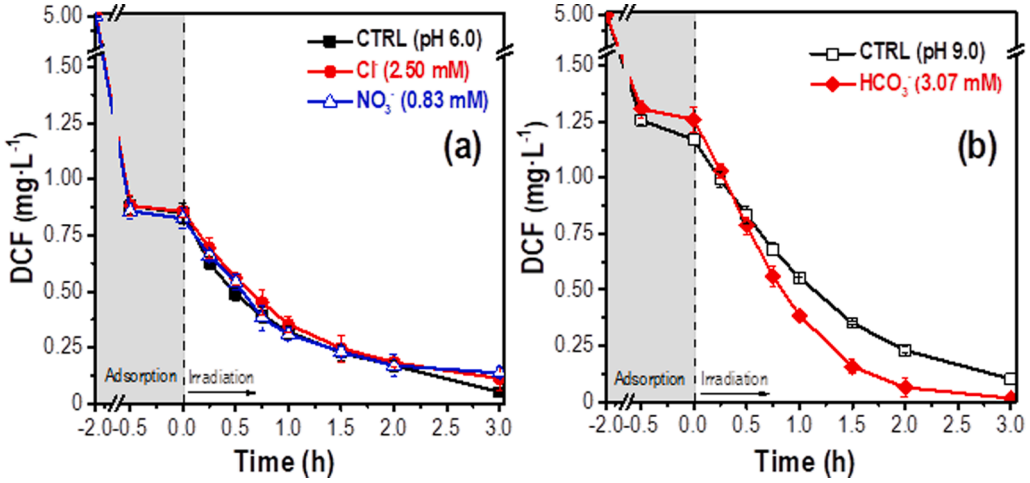

Fig. 8. Evolution of DCF concentration in the presence of (a) Cl^- and NO_3^- and (b) HCO_3^-. Photocatalyst (Ti2-C20) loading = 250 mg·L^{-1} and $[DCF]_0$ = 5 mg·L^{-1}.

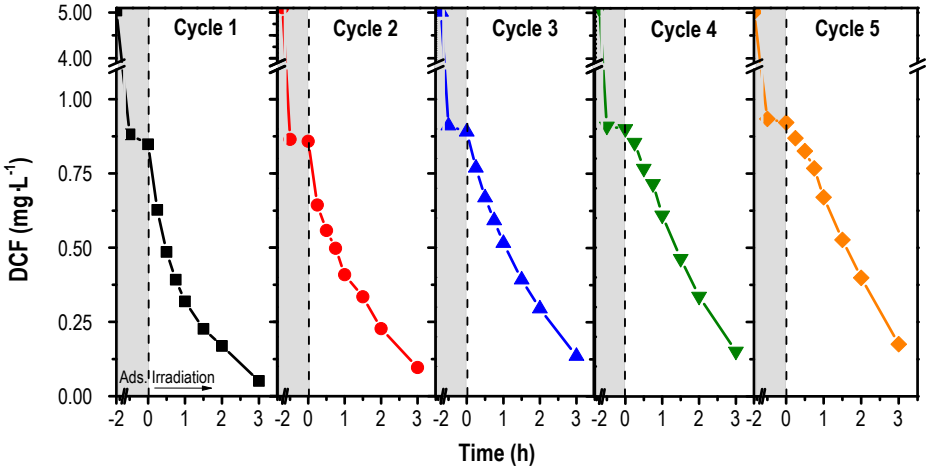

Fig. 9. Removal of DCF under simulated solar light using Ti2-C20 (250 mg·L^{-1}) for five consecutive cycles. $[DCF]_0$ = 5 mg·L^{-1} and pH_0 = 6.0.

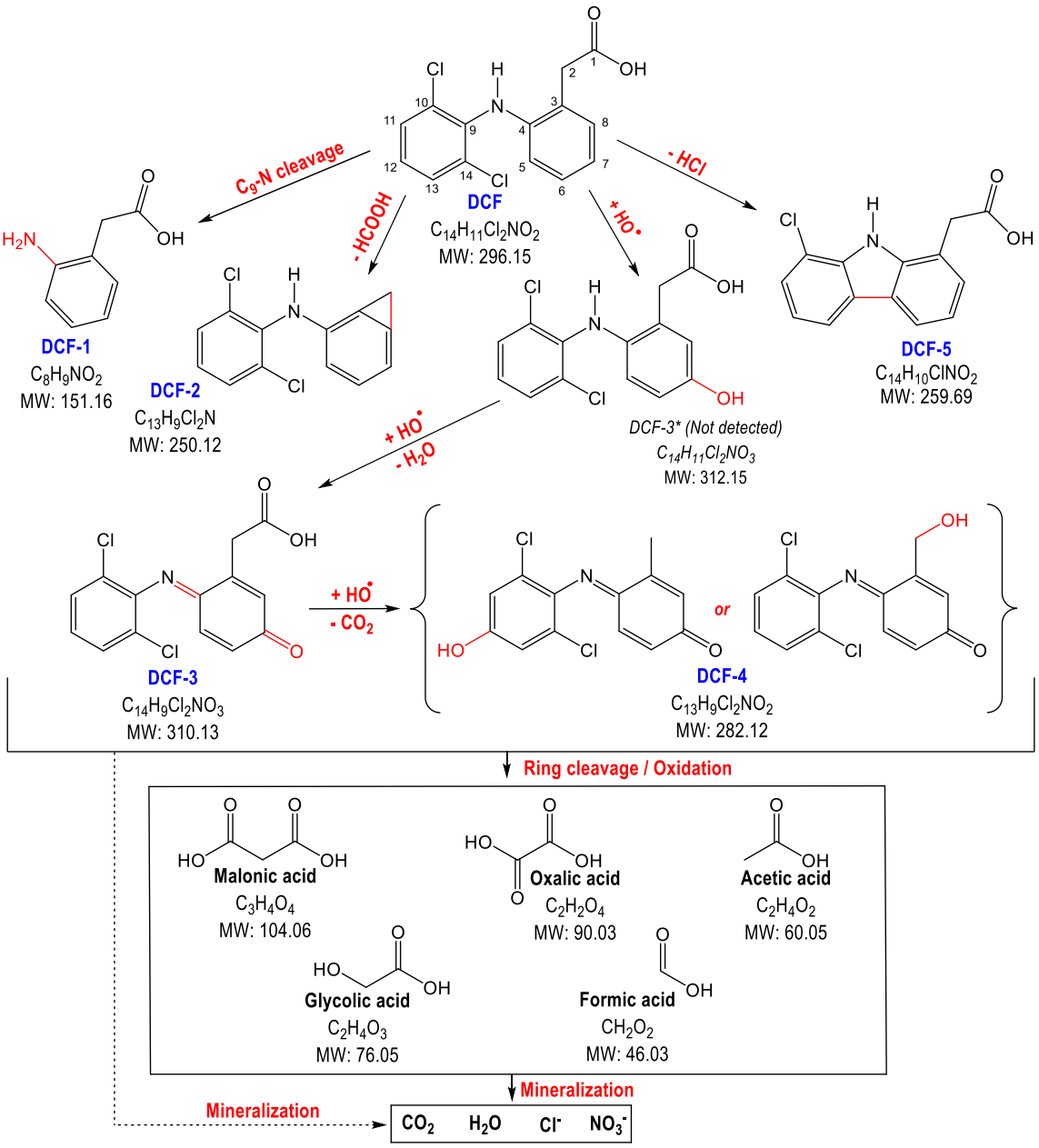

Fig. 10. Proposed photocatalytic degradation pathway of DCF under simulated solar light with Ti2-C20.

heterostructure and the counterpart after five cycles (Fig. S6a and b) as well as XRD patterns (Fig. S6c) did not show any appreciable difference in the morphology or anatase crystalline phase after the consecutive reuse. However, thermogravimetric analysis in air (Fig. S6d) showed a decrease (i.e., from 72.3 to 66.4%, respectively) in the residual material after calcination at 900 °C. Since the decrease occurs at temperatures higher than 500 °C it can be attributed to some loss of TiO_2. Therefore, the decrease of photocatalytic performance can be ascribed to a slight loss of the active phase after successive use (e.g., due to stirring) and recovery processes. However, given the overall photocatalytic degradation of the contaminant, it can be concluded that the Ti2-C20 catalyst shows a good structural and photocatalytic stability over reuse.

3.2.4. *DCF degradation byproducts and pathways*

The byproducts generated from the photocatalytic degradation of DCF under simulated solar light were tentatively identified by LC/ESI-MS and IC analyses. Table S4 summarizes the parameters obtained from LC/ESI-MS. Following low mass error (<-1 mDa) threshold in the analysis of LC/ESI-MS results of the detected masses allowed for high confidence level of the proposed degradation byproducts. Besides, the number of rings and double bonds (RDB) existing in a molecule was considered. For example, parent DCF has a RDB of 9, corresponding 8 to the aromatic rings (i.e., 4 each one, composed of the 3 double bonds and 1 from the ring itself) and the C=O double bond from the carboxylic acid group. Following this procedure, five organic byproducts were identified within the DCF photocatalytic degradation via four different oxidation routes (Fig. 10).

The first route would involve oxidative cleavage of the C_9–N bond with the formation of byproduct DCF-1 (*m/z* 152.0703). A similar pathway was reported for DCF photocatalytic degradation in water under visible light [48,50]. The evolution of this byproduct, depicted in Fig. 11a, shows that DCF-1 peaked in the first 60 min of irradiation and subsequently was removed. The second DCF degradation route would encompass loss of formic acid from C_2 followed by generation of DCF-2 (*m/z* 250.0181), as previously described by Calza et al. [51]. As shown in Fig. 11a, DCF-2 was only detected after 30 min of the photocatalytic

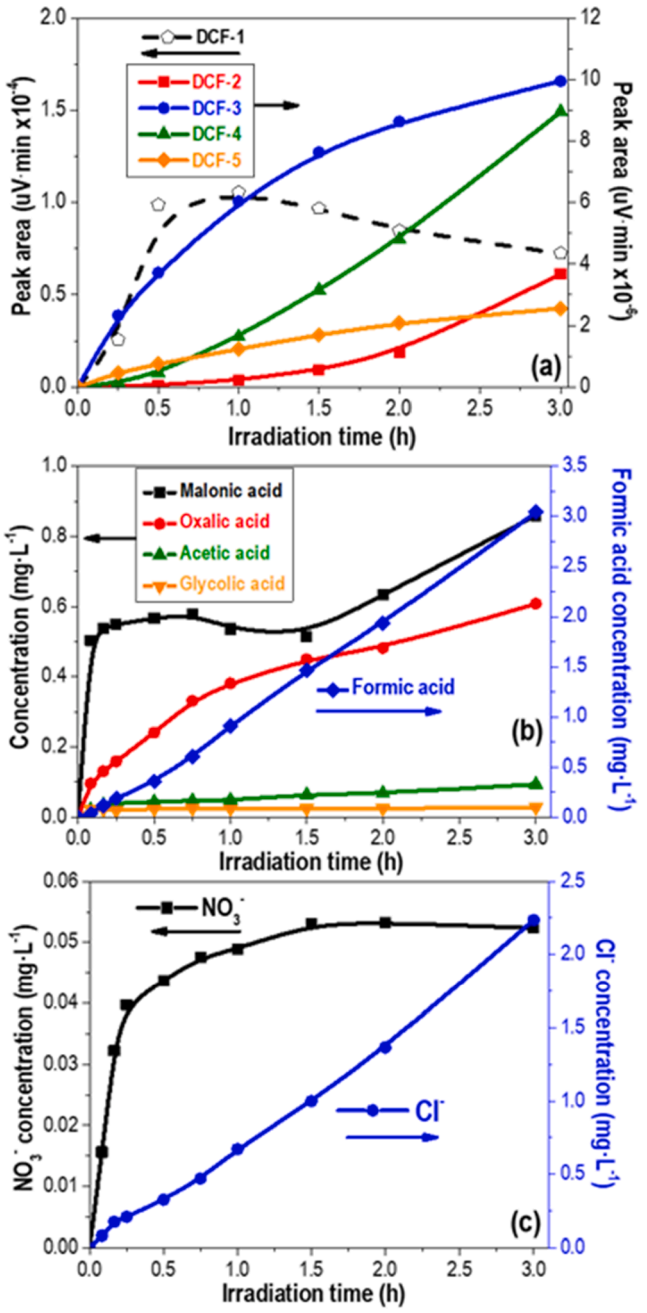

Fig. 11. (a) Evolution profile of reaction byproducts, (b) short-chain carboxylic acids and (c) inorganic anions (NO_3^- and Cl^-) in the photocatalytic degradation of DCF under simulated solar light with Ti2-C20 (250 mg·L^{-1}). $[DCF]_0 = 100$ mg·L^{-1} and $pH_0 = 6.0$.

reaction. The suggested loss of formic acid through this second route was further confirmed by the gradual accumulation of formic acid in the system as depicted in Fig. 11b. The third degradation route probably involve hydroxylation of the DCF aromatic ring at C_7 position, with the formation of a mono-hydroxylated byproduct (DCF-3*, not detected), accordingly to Salaeh el al. [52]. This last would undergoes dehydration followed by electronic rearrangement in the benzene ring with ethanoic group to subsequently generate a quinone-imine derivative byproduct DCF-3 (*m/z* 310.0028), as previously reported [51–53]. The successive decarboxylation of DCF-3 at C_2 followed by $HO^{\bullet}$ attack may result in the formation of byproduct DCF-4 (*m/z* 282.0079), as rationalized by Hu et al. [48]. In the current study, two isomers of DCF-4 are suggested to be formed depending on whether the hydroxylation occurs at C_2 or C_{12}. The fourth DCF degradation pathway probably involve oxidative dechlorination at C_{14} followed by cyclization between the C_5 and C_{14} with the generation of a carbazole derivative DCF-5 (*m/z* 260.0468), as previously described by Martinez et al. [54]. Dechlorination of DCF was confirmed by the accumulated Cl^- in the solution, Fig. 11c. About 10% reduction in the total stoichiometric chlorine of DCF was accumulated after 3 h of reaction.

Under the oxidative environment of the current photocatalytic system, aromatic rings opening of byproducts would occur and result in the formation of low molecular weight carboxylic byproducts. Fig. 11b depicts their evolution profiles during the degradation process. A total of five carboxylic acids were detected, including mainly formic, malonic and oxalic. Acetic and glycolic acids were also detected, but at lower concentrations. Besides this, the generated inorganic ions were monitored, including Cl^- (as explained earlier) and NO_3^- (Fig. 11c), the latter obtained from the successive oxidation of N atoms in the molecule. It is worth mentioning that the formation of nitrate was much faster than that of Cl^-, although the former achieved much lower concentration (i.e., 0.05 mg·L^{-1} after 3 h reaction). Nitrite (NO_2^-) was always below the detection limit (0.01 mg·L^{-1}).

4. Conclusions

Synthesis of carbon microspheres from lignin was accomplished via an innovative two-steps (Fe-activated HTC and pyrolysis) approach. Spherical carbon microspheres, with diameters in the range of 0.9–1.9 μm, were prepared by controlling HTC holding time. The microspheres encompassed large specific surface area and well-developed porous texture. Anatase TiO_2 was successfully anchored on those carbon microspheres by solvothermal synthesis. Thus, novel TiO_2-carbon microspheres with a uniform TiO_2 dispersion and absorption in the visible region were obtained. The removal of selected pharmaceuticals in water demonstrated Ti2-C20 to yield the best performance, in terms of apparent photonic efficiency and photocatalytic degradation. The photocatalytic performance of TiO_2-carbon heterostructures was not affected by the presence of common inorganic anions present in wastewater after reclamation treatment (such as chloride and nitrate), while a slight improvement was observed in presence of bicarbonate. The Ti2-C20 photocatalyst showed excellent photocatalytic performance for over three consecutive treatment cycles. The degradation of diclofenac was suggested to majorly occur via C-N bond cleavage, hydroxylation, internal cyclization, and decarboxylation pathways, being identified five reaction byproducts. Five short-chain carboxylic acids were accumulated in the system due to successive oxidation/ring opening of these byproducts. The current results revealed the value of TiO_2-carbon microspheres heterostructures as well-developed photocatalysts for the remediation of pharmaceuticals in water under different environmental conditions.

Declaration of Competing Interest

The authors declare that they have no known competing financial interests or personal relationships that could have appeared to influence the work reported in this paper.

Acknowledgements

This research was funded by the Spanish State Research Agency (PID2019-106186RB-I00/AEI/10.13039/501100011033). M. Peñas-Garzón is indebted to Spanish MECD for a FPU grant (FPU16/00576 grant) and to Spanish MICIU for funding the international stay (EST18/00048 grant) at the Department of Chemical and Environmental Engineering (ChEE), University of Cincinnati. Authors thank the Research Support Services of the University of Extremadura (SAIUEx) for its technical and scientific support.

Appendix A. Supplementary material

Supplementary data to this article can be found online at https://doi.org/10.1016/j.seppur.2021.119169.

References

[1] P. Sathishkumar, R.A.A. Meena, T. Palanisami, V. Ashokkumar, T. Palvannan, F. L. Gu, Occurrence, interactive effects and ecological risk of diclofenac in environmental compartments and biota - a review, Sci. Total Environ. 698 (2020), 134057, https://doi.org/10.1016/j.scitotenv.2019.134057.

[2] S. Fekadu, E. Alemayehu, R. Dewil, B. Van der Bruggen, Pharmaceuticals in freshwater aquatic environments: A comparison of the African and European challenge, Sci. Total Environ. 654 (2019) 324–337, https://doi.org/10.1016/j.scitotenv.2018.11.072.

[3] J. Diaz-Angulo, J. Porras, M. Mueses, R.A. Torres-Palma, A. Hernandez-Ramirez, F. Machuca-Martinez, Coupling of heterogeneous photocatalysis and photosensitized oxidation for diclofenac degradation: role of the oxidant species, J. Photochem. Photobiol. A Chem. 383 (2019), 112015, https://doi.org/10.1016/j.jphotochem.2019.112015.

[4] D. Kanakaraju, B.D. Glass, M. Oelgemöller, Advanced oxidation process-mediated removal of pharmaceuticals from water: A review, J. Environ. Manage. 219 (2018) 189–207, https://doi.org/10.1016/j.jenvman.2018.04.103.

[5] N.F.F. Moreira, C. Narciso-da-Rocha, M.I. Polo-López, L.M. Pastrana-Martínez, J. L. Faria, C.M. Manaia, P. Fernández-Ibáñez, O.C. Nunes, A.M.T. Silva, Solar treatment (H_2O_2, TiO_2-P25 and GO-TiO_2 photocatalysis, photo-Fenton) of organic micropollutants, human pathogen indicators, antibiotic resistant bacteria and related genes in urban wastewater, Water Res. 135 (2018) 195–206, https://doi.org/10.1016/j.watres.2018.01.064.

[6] S. Ghosh, H. Remita, R.N. Basu, Visible-light-induced reduction of Cr(VI) by PDPB-ZnO nanohybrids and its photo-electrochemical response, Appl. Catal. B Environ. 239 (2018) 362–372, https://doi.org/10.1016/j.apcatb.2018.08.034.

[7] M. Pelaez, N.T. Nolan, S.C. Pillai, M.K. Seery, P. Falaras, A.G. Kontos, P.S. M. Dunlop, J.W.J. Hamilton, J.A. Byrne, K. O'Shea, M.H. Entezari, D.D. Dionysiou, A review on the visible light active titanium dioxide photocatalysts for environmental applications, Appl. Catal. B Environ. 125 (2012) 331–349, https://doi.org/10.1016/j.apcatb.2012.05.036.

[8] H. Dong, G. Zeng, L. Tang, C. Fan, C. Zhang, X. He, Y. He, An overview on limitations of TiO_2-based particles for photocatalytic degradation of organic pollutants and the corresponding countermeasures, Water Res. 79 (2015) 128–146, https://doi.org/10.1016/j.watres.2015.04.038.

[9] M.F.J. Dijkstra, A. Michorius, H. Buwalda, H.J. Panneman, J.G.M. Winkelman, A.A. C.M. Beenackers, Comparison of the efficiency of immobilized and suspended systems in photocatalytic degradation, Catal. Today. 66 (2001) 487–494, https://doi.org/10.1016/S0920-5861(01)00257-7.

[10] S. Ghosh, S.R. Keshri, S. Bera, R.N. Basu, Enhanced solar hydrogen generation using Cu–Cu2O integrated polypyrrole nanofibers as heterostructured catalysts, Int. J. Hydrogen Energy. 45 (2020) 6159–6173, https://doi.org/10.1016/j.ijhydene.2019.12.118.

[11] E. Vesali-Kermani, A. Habibi-Yangjeh, S. Ghosh, Visible-light-induced nitrogen photofixation ability of g-C_3N_4 nanosheets decorated with MgO nanoparticles, J. Ind. Eng. Chem. 84 (2020) 185–195, https://doi.org/10.1016/j.jiec.2019.12.033.

[12] J. Liu, N.P. Wickramaratne, S.Z. Qiao, M. Jaroniec, Molecular-based design and emerging applications of nanoporous carbon spheres, Nat. Mater. 14 (2015) 763–774, https://doi.org/10.1038/nmat4317.

[13] H. Mao, X. Chen, R. Huang, M. Chen, R. Yang, P. Lan, M. Zhou, F. Zhang, Y. Yang, X. Zhou, Fast preparation of carbon spheres from enzymatic hydrolysis lignin: Effects of hydrothermal carbonization conditions, Sci. Rep. 8 (2018) 9501, https://doi.org/10.1038/s41598-018-27777-4.

[14] M.M. Titirici, M. Antonietti, N. Baccile, Hydrothermal carbon from biomass: A comparison of the local structure from poly- to monosaccharides and pentoses/hexoses, Green Chem. 10 (2008) 1204–1212, https://doi.org/10.1039/b807009a.

[15] N. Díez, M. Qiao, J.L. Gómez-Urbano, C. Botas, D. Carriazo, M.M. Titirici, High density graphene-carbon nanosphere films for capacitive energy storage, J. Mater. Chem. A. 7 (2019) 6126–6133, https://doi.org/10.1039/c8ta12050a.

[16] J. Matos, A. García, L. Zhao, M.M. Titirici, Solvothermal carbon-doped TiO_2 photocatalyst for the enhanced methylene blue degradation under visible light, Appl. Catal. A Gen. 390 (2010) 175–182, https://doi.org/10.1016/j.apcata.2010.10.009.

[17] V.K. Ponnusamy, D.D. Nguyen, J. Dharmaraja, S. Shobana, J.R. Banu, R. G. Saratale, S.W. Chang, G. Kumar, A review on lignin structure, pretreatments, fermentation reactions and biorefinery potential, Bioresour. Technol. 271 (2019) 462–472, https://doi.org/10.1016/j.biortech.2018.09.070.

[18] J.J. Rodríguez, T. Cordero, J. Rodríguez-Mirasol, Carbon Materials from Lignin and Their Applications, in: Z. Fang, R.L. Smith (Eds.), Prod. Biofuels Chem. from Lignin. Biofuels Biorefineries, Springer, 2016: pp. 217–262. doi:10.1007/978-981-10-1965-4_8.

[19] C. Fernandez-Ruiz, J. Bedia, P. Bonal, J.J. Rodriguez, L.M. Gómez-Sainero, Chloroform conversion into ethane and propane by catalytic hydrodechlorination with Pd supported on activated carbons from lignin, Catal. Sci. Technol. 8 (2018) 3926–3935, https://doi.org/10.1039/c8cy00461g.

[20] G. Singh, K.S. Lakhi, S. Sil, S.V. Bhosale, I.Y. Kim, K. Albahily, A. Vinu, Biomass derived porous carbon for CO_2 capture, Carbon N. Y. 148 (2019) 164–186, https://doi.org/10.1016/j.carbon.2019.03.050.

[21] F.J. García-Mateos, R. Ruiz-Rosas, J. María Rosas, E. Morallón, D. Cazorla-Amorós, J. Rodríguez-Mirasol, T. Cordero, Activation of electrospun lignin-based carbon fibers and their performance as self-standing supercapacitor electrodes, Sep. Purif. Technol. 241 (2020), https://doi.org/10.1016/j.seppur.2020.116724.

[22] D. Choi, H.S. Kil, S. Lee, Fabrication of low-cost carbon fibers using economical precursors and advanced processing technologies, Carbon N. Y. 142 (2019) 610–649, https://doi.org/10.1016/j.carbon.2018.10.028.

[23] D. Saha, K.E. Warren, A.K. Naskar, Soft-templated mesoporous carbons as potential materials for oral drug delivery, Carbon N. Y. 71 (2014) 47–57, https://doi.org/10.1016/j.carbon.2014.01.005.

[24] A. Gómez-Avilés, M. Peñas-Garzón, J. Bedia, J.J. Rodriguez, C. Belver, C-modified TiO_2 using lignin as carbon precursor for the solar photocatalytic degradation of acetaminophen, Chem. Eng. J. 358 (2019) 1574–1582, https://doi.org/10.1016/j.cej.2018.10.154.

[25] M. Peñas-Garzón, A. Gómez-Avilés, J. Bedia, J.J. Rodriguez, C. Belver, Effect of activating agent on the properties of TiO_2/activated carbon heterostructures for solar photocatalytic degradation of acetaminophen, Materials (Basel). 12 (2019) 378–404, https://doi.org/10.3390/ma12030378.

[26] M. Peñas-Garzón, A. Gómez-Avilés, C. Belver, J.J. Rodriguez, J. Bedia, Degradation pathways of emerging contaminants using TiO_2-activated carbon heterostructures in aqueous solution under simulated solar light, Chem. Eng. J. 392 (2020), 124867, https://doi.org/10.1016/j.cej.2020.124867.

[27] Z. Xu, Y. Zhou, Z. Sun, D. Zhang, Y. Huang, S. Gu, W. Chen, Understanding reactions and pore-forming mechanisms between waste cotton woven and $FeCl_3$ during the synthesis of magnetic activated carbon, Chemosphere. 241 (2020), 125120, https://doi.org/10.1016/j.chemosphere.2019.125120.

[28] S. Brunauer, P.H. Emmett, E. Teller, Adsorption of Gases in Multimolecular Layers, J. Am. Chem. Soc. 60 (1938) 309–319, https://doi.org/10.1021/ja01269a023.

[29] B.C. Lippens, de B. J.H, Studies on pore systems in catalysts: V. The t method, J. Catal. 4 (1965) 319–323, https://doi.org/10.1016/0021-9517(65)90307-6.

[30] J. Tauc, Absorption edge and internal electric fields in amorphous semiconductors, Mater. Res. Bull. 5 (1970) 721–729, https://doi.org/10.1016/0025-5408(70)90112-1.

[31] J. Zhang, P. Zhou, J. Liu, J. Yu, New understanding of the difference of photocatalytic activity among anatase, rutile and brookite TiO_2, Phys. Chem. Chem. Phys. 16 (2014) 20382–20386, https://doi.org/10.1039/c4cp02201g.

[32] G. Newcombe, R. Hayes, M. Drikas, Granular activated carbon: Importance of surface properties in the adsorption of naturally occurring organics, Colloids Surfaces A Physicochem. Eng. Asp. 78 (1993) 65–71, https://doi.org/10.1016/0927-7757(93)80311-2.

[33] W.H.M. Abdelraheem, M.N. Nadagouda, D.D. Dionysiou, Solar light-assisted remediation of domestic wastewater by NB-TiO_2 nanoparticles for potable reuse, Appl. Catal. B Environ. 269 (2020), 118807, https://doi.org/10.1016/j.apcatb.2020.118807.

[34] C. Falco, N. Baccile, M.M. Titirici, Morphological and structural differences between glucose, cellulose and lignocellulosic biomass derived hydrothermal carbons, Green Chem. 13 (2011) 3273–3281, https://doi.org/10.1039/c1gc15742f.

[35] O. Carp, C.L. Huisman, A. Reller, Photoinduced reactivity of titanium dioxide, Prog. Solid State Chem. 32 (2004) 33–177, https://doi.org/10.1016/j.progsolidstchem.2004.08.001.

[36] M. Thommes, K. Kaneko, A.V. Neimark, J.P. Olivier, F. Rodriguez-Reinoso, J. Rouquerol, K.S.W. Sing, Physisorption of gases, with special reference to the evaluation of surface area and pore size distribution (IUPAC Technical Report), Pure Appl. Chem. 87 (2015) 1051–1069, https://doi.org/10.1515/pac-2014-1117.

[37] J. Bedia, C. Belver, S. Ponce, J. Rodriguez, J.J. Rodriguez, Adsorption of antipyrine by activated carbons from $FeCl_3$-activation of Tara gum, Chem. Eng. J. 333 (2018) 58–65, https://doi.org/10.1016/j.cej.2017.09.161.

[38] H. Wu, X.L. Wu, Z.M. Wang, H. Aoki, S. Kutsuna, K. Jimura, S. Hayashi, Anchoring titanium dioxide on carbon spheres for high-performance visible light photocatalysis, Appl. Catal. B Environ. 207 (2017) 255–266, https://doi.org/10.1016/j.apcatb.2017.02.027.

[39] P. Makuła, M. Pacia, W. Macyk, How To Correctly Determine the Band Gap Energy of Modified Semiconductor Photocatalysts Based on UV-Vis Spectra, J. Phys. Chem. Lett. 9 (2018) 6814–6817, https://doi.org/10.1021/acs.jpclett.8b02892.

[40] G. Zhang, Y.C. Zhang, M. Nadagouda, C. Han, K. O'Shea, S.M. El-Sheikh, A. A. Ismail, D.D. Dionysiou, Visible light-sensitized S, N and C co-doped polymorphic TiO2 for photocatalytic destruction of microcystin-LR, Appl. Catal. B Environ. 144 (2014) 614–621, https://doi.org/10.1016/j.apcatb.2013.07.058.

[41] W.H.M. Abdelraheem, M.K. Patil, M.N. Nadagouda, D.D. Dionysiou, Hydrothermal synthesis of photoactive nitrogen- and boron- codoped TiO_2 nanoparticles for the treatment of bisphenol A in wastewater: Synthesis, photocatalytic activity, degradation byproducts and reaction pathways, Appl. Catal. B Environ. 241 (2019) 598–611, https://doi.org/10.1016/j.apcatb.2018.09.039.

[42] Y.O. Donar, S. Bilge, A. Sınağ, O. Pliekhov, TiO_2/Carbon Materials Derived from Hydrothermal Carbonization of Waste Biomass: A Highly Efficient, Low-Cost Visible-Light-Driven Photocatalyst, ChemCatChem. 10 (2018) 1134–1139, https://doi.org/10.1002/cctc.201701405.

[43] L. Zhao, X. Chen, X. Wang, Y. Zhang, W. Wei, Y. Sun, M. Antonietti, M.M. Titirici, One-step solvothermal synthesis of a carbon @TiO_2 dyade structure effectively promoting visible-light photocatalysis, Adv. Mater. 22 (2010) 3317–3321, https://doi.org/10.1002/adma.201000660.

[44] John F. Moulder, Handbook of X-ray Photoelectron Spectroscopy: A Reference Book of Standard Spectra for Identification and Interpretation of XPS Data, Physical E, 1995. https://books.google.com.mx/books?id=fjqtQAAACAAJ (accessed May 25, 2021).
[45] G. An, W. Ma, Z. Sun, Z. Liu, B. Han, S. Miao, Z. Miao, K. Ding, Preparation of titania/carbon nanotube composites using supercritical ethanol and their photocatalytic activity for phenol degradation under visible light irradiation, Carbon N. Y. 45 (2007) 1795–1801, https://doi.org/10.1016/j.carbon.2007.04.034.
[46] J. Zhu, F. Chen, J. Zhang, H. Chen, M. Anpo, Fe3+-TiO2 photocatalysts prepared by combining sol-gel method with hydrothermal treatment and their characterization, J. Photochem. Photobiol. A Chem. 180 (2006) 196–204, https://doi.org/10.1016/j.jphotochem.2005.10.017.
[47] A.R. Lado Ribeiro, N.F.F. Moreira, G. Li Puma, A.M.T. Silva, Impact of water matrix on the removal of micropollutants by advanced oxidation technologies, Chem. Eng. J. 363 (2019) 155–173, https://doi.org/10.1016/j.cej.2019.01.080.
[48] Z. Hu, X. Cai, Z. Wang, S. Li, Z. Wang, X. Xie, Construction of carbon-doped supramolecule-based g-C_3N_4/TiO_2 composites for removal of diclofenac and carbamazepine: A comparative study of operating parameters, mechanisms, degradation pathways, J. Hazard. Mater. 380 (2019), 120812, https://doi.org/10.1016/j.jhazmat.2019.120812.
[49] Y. Huang, M. Kong, D. Westerman, E.G. Xu, S. Coffin, K.H. Cochran, Y. Liu, S. D. Richardson, D. Schlenk, D.D. Dionysiou, Effects of HCO_3^- on Degradation of Toxic Contaminants of Emerging Concern by UV/NO_3^-, Environ. Sci. Technol. 52 (2018) 12697–12707, https://doi.org/10.1021/acs.est.8b04383.
[50] M. Cai, R. Li, Z. Xie, J. Huang, Y. Zeng, Q. Zhang, H. Liu, W. Lv, G. Liu, Synthesis of a core-shell heterostructured MoS_2/$Cd_{0.9}Zn_{0.1}S$ photocatalyst for the degradation of diclofenac under visible light, Appl. Catal. B Environ. 259 (2019), 118033, https://doi.org/10.1016/j.apcatb.2019.118033.
[51] P. Calza, V.A. Sakkas, C. Medana, C. Baiocchi, A. Dimou, E. Pelizzetti, T. Albanis, Photocatalytic degradation study of diclofenac over aqueous TiO_2 suspensions, Appl. Catal. B Environ. 67 (2006) 197–205, https://doi.org/10.1016/j.apcatb.2006.04.021.
[52] S. Salaeh, D. Juretic Perisic, M. Biosic, H. Kusic, S. Babic, U. Lavrencic Stangar, D. D. Dionysiou, A. Loncaric Bozic, Diclofenac removal by simulated solar assisted photocatalysis using TiO_2-based zeolite catalyst; mechanisms, pathways and environmental aspects, Chem. Eng. J. 304 (2016) 289–302, https://doi.org/10.1016/j.cej.2016.06.083.
[53] S. Murgolo, I.S. Moreira, C. Piccirillo, P.M.L. Castro, G. Ventrella, C. Cocozza, G. Mascolo, Photocatalytic degradation of diclofenac by hydroxyapatite-TiO_2 composite material: Identification of transformation products and assessment of toxicity, Materials (Basel). 11 (2018) 1779, https://doi.org/10.3390/ma11091779.
[54] C. Martínez, M. Canle L, M.I. Fernández, J.A. Santaballa, J. Faria, Aqueous degradation of diclofenac by heterogeneous photocatalysis using nanostructured materials, Appl. Catal. B Environ. 107 (2011) 110–118, https://doi.org/10.1016/j.apcatb.2011.07.003.